Progress in Biophysics and Molecular Biology 107 (2011) 101–111

Contents lists available at ScienceDirect

Progress in Biophysics and Molecular Biology

journal homepage: www.elsevier.com/locate/pbiomolbio

Original Research

Experiment-model interaction for analysis of epicardial activation during human ventricular fibrillation with global myocardial ischaemia

R.H. Clayton [a,*], M.P. Nash [b,c], C.P. Bradley [b,d], A.V. Panfilov [e], D.J. Paterson [d], P. Taggart [f]

[a] Department of Computer Science, University of Sheffield, Regent Court, 211 Portobello, S1 4DP, UK
[b] Bioengineering Institute, University of Auckland, New Zealand
[c] Engineering Science, University of Auckland, New Zealand
[d] Department of Physiology, Anatomy and Genetics, University of Oxford, UK
[e] Department of Physics and Astronomy, Ghent University, Belgium
[f] Departments of Cardiology and Cardiothoracic Surgery, University College Hospital, London, UK

ARTICLE INFO

Article history:
Available online 2 July 2011

Keywords:
Ventricular fibrillation
Ischaemia
Re-entry
Computer model

ABSTRACT

We describe a combined experiment-modelling framework to investigate the effects of ischaemia on the organisation of ventricular fibrillation in the human heart. In a series of experimental studies epicardial activity was recorded from 10 patients undergoing routine cardiac surgery. Ventricular fibrillation was induced by burst pacing, and recording continued during 2.5 min of global cardiac ischaemia followed by 30 s of coronary reflow. Modelling used a 2D description of human ventricular tissue. Global cardiac ischaemia was simulated by (i) decreased intracellular ATP concentration and subsequent activation of an ATP sensitive K^+ current, (ii) elevated extracellular K^+ concentration, and (iii) acidosis resulting in reduced magnitude of the L-type Ca^{2+} current $I_{Ca,L}$. Simulated ischaemia acted to shorten action potential duration, reduce conduction velocity, increase effective refractory period, and flatten restitution. In the model, these effects resulted in slower re-entrant activity that was qualitatively consistent with our observations in the human heart. However, the flattening of restitution also resulted in the collapse of many re-entrant waves to several stable re-entrant waves, which was different to the overall trend we observed in the experimental data. These findings highlight a potential role for other factors, such as structural or functional heterogeneity in sustaining wavebreak during human ventricular fibrillation with global myocardial ischaemia.

1. Introduction

Computational models of cardiac electrophysiology have made an important contribution to our understanding of the mechanisms that initiate and sustain cardiac arrhythmias. In particular, these models have highlighted the role played by re-entry, in which an activation wavefront rotates by propagating continually into recovering tissue.

Ventricular fibrillation (VF) is a potentially lethal cardiac arrhythmia, and experimental evidence from animal studies indicates that VF is sustained by re-entry. However, although there are many data from animal hearts, there are only a few studies that describe in detail the electrical activation sequence during VF in the human heart (Nanthakumar et al., 2004; Masse et al., 2007, 2009; Nash et al., 2006b; Walcott et al., 2002; Wu et al., 1998).

Interpretation of data from the in-situ human heart is difficult, because the clinical context limits what information can be recorded. For example in our own studies of human VF we have recorded epicardial electrograms (Nash et al., 2006b), but we could not record transmural or endocardial activation, and it is not easy to determine detailed electrophysiological properties such as action potential duration (APD) restitution (Nash et al., 2006a) at the same time as a VF study. For these reasons, computational models of cell, tissue, and whole organ electrophysiology are valuable tools for mechanistic interpretation of VF recordings, because it is possible to examine how parameters that operate at the cell scale (for example the maximum conductance of an ion channel or change in cell environment) influence patterns of electrical activation at the tissue and whole organ scales, and to assess whether the activation patterns in a simulation are consistent with surface activation patterns recorded from a human heart (Keldermann et al., 2008,

* Corresponding author. Tel.: +44 114 222 1845; fax: +44 114 222 1810.
E-mail address: r.h.clayton@sheffield.ac.uk (R.H. Clayton).

0079-6107/$ – see front matter © 2011 Elsevier Ltd. All rights reserved.
doi:10.1016/j.pbiomolbio.2011.06.010

2009; Ten Tusscher et al., 2009). In order to have maximal impact, modelling should be based upon and verified against experimental studies of the same process. This approach confines possible parameter choices and simulation protocols in modelling, and so produces results that complement experimental work.

In this paper, we focus on how acute global cardiac ischaemia modifies the mechanisms that sustain human VF. Our data from human hearts were obtained in studies where we mapped epicardial activation during VF with global cardiac ischaemia resulting from occluded coronary flow, but where it was not practical (or ethical) to control the extent and depth of ischaemia. Re-entry is an important arrhythmia mechanism that acts to sustain VF. In the present study we have therefore used a computational model of human ventricular tissue to examine how simulated ischaemia at the cell level influences the behaviour of re-entry at the tissue level, and to link these simulation results with our experimental recordings. We aim to examine how a model of ischaemia that uses simplified tissue geometry and simplified representation of ischaemia can provide insight into experimental results.

2. Ventricular fibrillation and global cardiac ischaemia

2.1. Background

Following initiation of spontaneous VF, perfusion of the myocardium is interrupted and global myocardial ischaemia begins to influence the activation patterns of VF. This effect is distinct from regional ischaemia resulting from occlusion of a single coronary artery because it affects the entire heart. This natural progression of VF was first studied in detail in canine hearts (Wiggers, 1940), where a trend to slower and more fragmented mechanical activity was observed before contraction ceased altogether. More recent studies in animal hearts have sought to quantify the characteristics of long duration VF by mapping electrical activity and identifying the number of re-entrant waves. Studies in rabbit, canine and porcine hearts have shown that during the first minutes of global cardiac ischaemia there was an initial increase in VF activation frequency and the number of activation waves followed by a steady decrease, and that this trend was accompanied by a steady decrease in conduction velocity (CV) (Huang et al., 2004; Huizar et al., 2007; Mandapati et al., 1998; Wu et al., 2002; Warren et al., 2007). After more than 3 min of ischaemia, there is evidence from studies in animal hearts that focal activity originating in the endocardium may play an increasing role in sustaining VF (Kong et al., 2009; Li et al., 2008; Venable et al., 2010), and that after 5 min of ischaemia increased gap junction resistance begins to both slow and block conduction (De Groot and Coronel, 2004).

The changes in cardiac cell and tissue electrophysiology that result from ischaemia are the consequence of a complex metabolic response (Carmeliet, 1999). The time course of these changes results mainly from (i) a gradual fall in $[ATP]_i$ of around 0.2 mM per minute (Weiss et al., 1992; Befroy et al., 1999) as a consequence of anoxia, which activates ATP sensitive K^+ channels resulting in an additional outward K^+ current, (ii) a rapid rise in $[K^+]_o$ from a normal value of around 4.0 mM of between 0.5 and 1 mM per minute (Janse and Wit, 1989), which alters outward K^+ currents and elevates the resting potential of the cell, and (iii) a fall in intracellular pH from a normal value of around 7 of around 0.1 units per minute (acidosis) that influences the inward rectifier K^+ current I_{K1}, the L-type Ca^{2+} current $I_{Ca,L}$, and intracellular Ca^{2+} handling (Carmeliet, 1999; Kodama et al., 1984; Wilde et al., 1988). All of these effects combine to reduce excitability and conduction velocity (CV), shorten APD, increase effective refractory period, and flatten APD restitution (Huang et al., 2004; Huizar et al., 2007; Warren et al., 2007).

The steepness of the APD restitution curve influences the stability of re-entry (Weiss et al., 2000), although modelling studies have shown that several other mechanisms can also act to destabilise re-entry (Fenton et al., 2002). An APD restitution curve with a steepness of >1 will tend to amplify any differences in APD along a wavefront, leading to instability and wavebreaks. Experimental studies in human hearts indicate that cardiac ischaemia acts to slow conduction, shorten APD, flatten APD restitution, and prolong refractoriness (Taggart et al., 1996). This effect, combined with a reduction in excitability during ischaemia (Wu et al., 2002) provides a mechanistic interpretation for the transition to slower activity with fewer wavefronts during ischaemic VF.

2.2. Experimental clinical studies in the human heart

We mapped epicardial electrical activity in ten patients undergoing routine cardiac surgery with global cardiac ischaemia and reperfusion, and these studies are described in detail elsewhere (Bradley et al., in press). Briefly, VF was induced by burst pacing while the patients were on cardiopulmonary bypass, maintaining cerebral and systemic perfusion. Epicardial activity was mapped by recording unipolar epicardial electrograms using a sock with 256 electrodes fitted over the left and right ventricles. The spacing between electrodes was approximately 10 mm, and the signal from each electrode was recorded at a sampling rate of 1 kHz. After a 30 s period of VF with coronary perfusion, global cardiac ischaemia was induced by aortic cross clamp and then maintained for 180 s, followed by release of the cross clamp and coronary reflow for a further 30 s.

The electrogram voltage was interpolated over the epicardial surface, transformed into phase using a Hilbert transform, and these data were then used to identify phase singularities (PS) at the ends of re-entrant waves and wavefronts as described previously (Nash et al., 2006b). A summary of our experimental findings is shown in Fig. 1, a much more detailed analysis is presented elsewhere (Bradley et al., in press).

The top panel of Fig. 1 shows dominant frequency (DF), which is the frequency of the dominant peak in the spectrum of electrogram signals and can be considered to be the inverse of local activation periods (Mandapati et al., 1998; Nash et al., 2006b). In our data there was an initial increase in DF followed by a slowing as ischaemia progresses, consistent with the studies in animal hearts described above. However, these studies in animal hearts would also predict a simultaneous reduction in the number of wavefronts during ischaemia. In contrast, we observed an initial steep increase in the number of PS and wavefronts during coronary perfusion, followed by a continuing increase in the number of wavefronts and the number of PS during global cardiac ischaemia (Fig. 1b and c). Despite the scatter of these points, statistical analysis with a linear mixed effects model showed these changes to be significant (Bradley et al., in press). During coronary reflow we found a rapid increase in activation rate, but no significant change in the number of wavefronts and PS.

2.3. Aim of the present study

Our overall aim in this study was to examine how global myocardial ischaemia modifies the behaviour of re-entry in the human ventricles using a computational model, and so to propose candidate explanations for the findings described above. Models are inevitably a simplified representation of real systems. The ability to control complexity is a powerful aspect of models when used as experimental tools because the model can be simplified in ways that would be difficult or impossible experimentally. Following the principle of Occam's razor, a model used to address

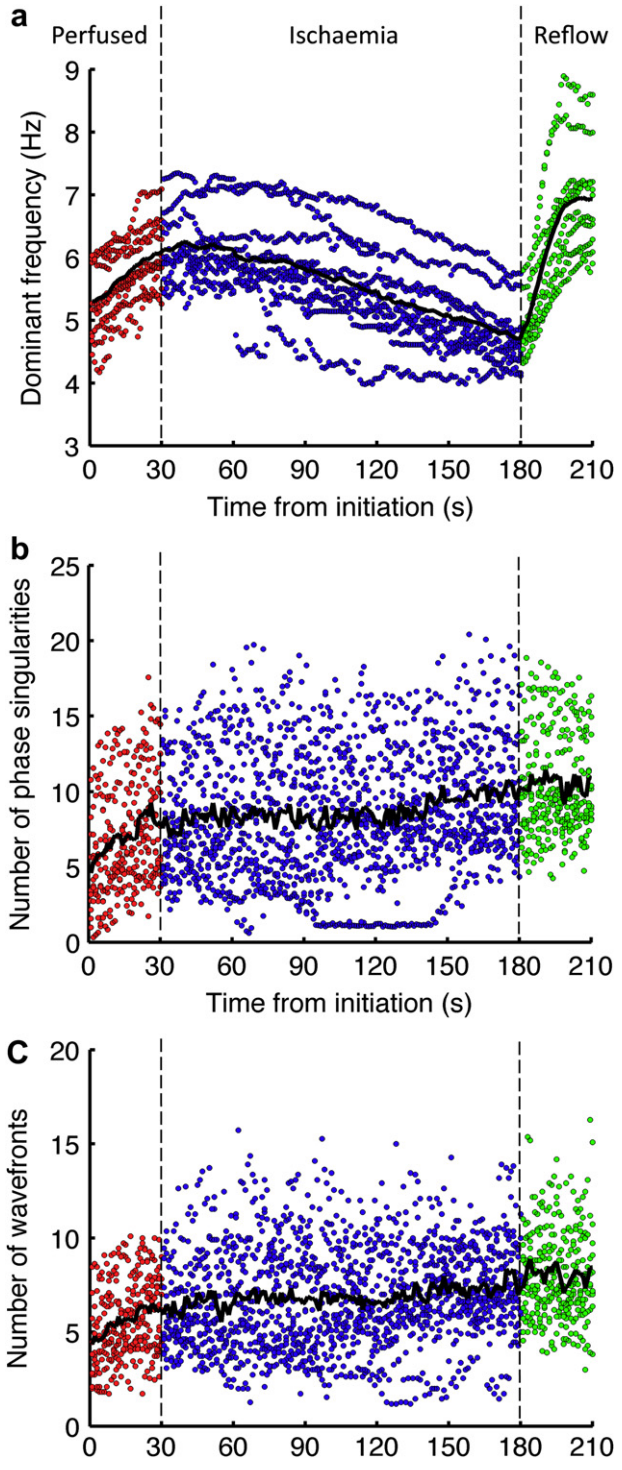

Fig. 1. (colour in print and on web) Summary of experimental data (see Bradley et al., in press for details). Each plot shows data from 10 patients, with each point showing the average value in a 1 s window for a single patient. Red points indicate perfused VF, blue ischaemic VF, and green reflow. Black line shows mean of the points. (a) Mean dominant frequency averaged over all electrodes, (b) number of phase singularities, and (c) number of wavefronts.

a specific research question should be as simple as possible but as complex as necessary, and for this study we simplified our representation of the human heart in three ways.

First, previous studies have simulated the metabolic response to ischaemia at the cell level (Michailova et al., 2007; Terkildsen et al., 2007), however the computational cost of embedding these cell scale models in a tissue level model is extremely high. We therefore chose to impose activation of ATP sensitive $[K^+]$ channels, elevated $[K^+]_o$, and the reduction of $I_{Ca,L}$ on our cell model (Nickerson and Buist, 2008; Ferrero et al., 1996, 2003; Shaw and Rudy, 1997; Warren et al., 2007), and then to examine how these changes influenced electrical activation and recovery in cardiac tissue (Ferrero et al., 2003; Rodríguez et al., 2004). This approach can be described as "middle out" (Noble, 2002) because our cell model does not provide a fully mechanistic description of ischaemia. Rather, we imposed the known consequences of ischaemia (such as elevated $[K^+]_o$) on the cell scale model, and examined the tissue level consequences of these changes.

Second, our human VF data are surface measurements of activation in the 3D ventricular wall, where tissue anisotropy and anatomy play a role in determining activation and recovery. Although simulations of human cardiac electrophysiology in anatomically detailed 3D geometry are possible (Ten Tusscher et al., 2009), our focus in the present study was the effect of simulated ischaemia on re-entry, and so we chose to strip away the complexity of 3D anisotropic tissue and to concentrate on re-entry in 2D tissue sheets. The computational cost of 2D simulations is lower, and many of the mechanisms that operate in 3D can be studied in 2D (Garny et al., 2005). However, there are limitations to this approach because some mechanisms operate in 3D fibrillation that are not present in 2D (Clayton, 2009).

Third, our experimental data for global cardiac ischaemia extend over a time period of 2.5 min. To simulate in detail the natural progression of ischaemia over this period, we would need to make assumptions about the time course of changes in the different components of ischaemia, and the computational such long duration simulations would be high. We therefore opted to take snapshots of ischaemia, represented by combinations of parameter values, and examined the behaviour of re-entry under these conditions. By setting the initial conditions of the model to be either a single re-entrant wave, or multiple wavelet re-entry, we were able to investigate how re-entry was modified by simulated ischaemia.

3. Methods

3.1. Cell model and simulated ischaemia

We used the Ten Tusscher Panfilov 2006 (TP06) model to represent human cellular electrophysiology (Ten Tusscher et al., 2004; Ten Tusscher and Panfilov, 2006). Although more detailed models for human ventricular cells have been developed recently (Grandi et al., 2010), we opted to use the TP06 model because it offers a compromise between biophysical detail and computational tractability. We used the parameters for epicardial cells as described in the TP06 paper, with modifications to simulate ischaemia that are described in detail below. We investigated the effects of $[ATP]_i$ depletion, $[K^+]_o$ accumulation, and acidosis independently.

Several formulations of the ATP activated K^+ current $I_{K,ATP}$ have been developed (Ferrero et al., 1996; Matsuoka et al., 2003; Shaw and Rudy, 1997; Michailova et al., 2007), but these are not based on data from human hearts. We chose to use the formulation described by Shaw and Rudy (1997) because this formulation has a greater influence than others for modest changes in $[ATP]_i$ (Nickerson and Buist, 2008):

$$I_{K,ATP} = G_{K,ATP} \frac{1}{1 + \left(\frac{[ATP]_i}{K_{0.5}}\right)^H} \left(\frac{[K^+]_o}{5.4}\right)^n (V_m - E_k) \quad (1)$$

Here V_m and E_K are the membrane voltage and reversal potential for K^+ ions respectively. $G_{K,ATP}$ is the maximum conductance of this current, set to 3.9 nS cm^{-2} similar to the values used in other computational studies of 4.0 mS cm^{-2} (Nickerson and Buist, 2008) and 3.4 mS cm^{-2} (Weiss et al., 2009), H is a Hill coefficient set to 2.0, and n was set to 0.24 (Shaw and Rudy, 1997). $[ATP]_i$ is intracellular ATP concentration, with a value in normal tissue of 6.8 mM, and $K_{0.5}$ the half maximal saturation of $I_{K,ATP}$, with a value in normal tissue of 0.043 mM (Ferrero et al., 1996). With these parameter values $I_{K,ATP}$ tends towards zero.

During ischaemia $[ATP]_i$ decreases slowly and activates $I_{K,ATP}$. In small mammals the fall in $[ATP]_i$ is around 0.2 mM per minute (Weiss et al., 1992; Befroy et al., 1999), but the rapid activity of VF may result in higher metabolic demand and a faster fall in $[ATP]_i$ in the human heart (Jessen et al., 1996), so we varied $[ATP]_i$ from a normal value of 6.8 mM to a reduced value of 4.0 mM. We assumed $K_{0.5}$ to vary linearly with $[ATP]_i$, so this parameter was varied between 0.043 mM for a normal value $[ATP]_i$ of 6.8 mM, and 0.306 mM for reduced $[ATP]_i$ of 4.0 mM. The Hill coefficient H was set to 2.0 and n to 0.24 (Shaw and Rudy, 1997).

We elevated $[K^+]_o$ from its default value of 5.4 mM to values between 6.0 and 9.5 mM. As noted above, $[K^+]_o$ increases by between 0.5 and 1 mM per minute of ischaemia (Janse and Wit, 1989; Weiss et al., 1992), and so these values would be typical for up to 3–6 min of ischaemia. Above 9.5 mM conduction velocity (CV) fell below 0.2 m s^{-1}, and above 12.0 mM conduction blocked.

The effect of acidosis was simulated by decreasing the maximum conductance of the L-type Ca^{2+} current GCa_L to 90% and 80% of its default value. A previous modelling study in which the TP06 model was used to investigate ischaemia (Nickerson and Buist, 2008) indicated that other effects of acidosis including changes to the inward rectifier K^+ current I_{K1}, the Na^+–Ca^{2+} exchanger I_{NaCa}, Ca^{2+} release from the sarcoplasmic reticulum, and Ca^{2+} uptake into the sarcoplasmic reticulum, have only a modest influence on the simulated action potential, so these changes were not included in the present study.

3.2. Tissue model and numerical approach

To determine restitution properties and examine re-entry, we used a 2D monodomain tissue model embedding the TPO6 cell model described above (Clayton et al., 2011), with isotropic diffusion, a diffusion coefficient of 1.171 cm^2 s^{-1}, and specific capacitance of 1 μF cm^{-2}. This model was solved using an explicit finite difference scheme with a space step of 0.025 cm, and adaptive time stepping (Qu and Garfinkel, 1999) with a time step between 0.02 and 0.1 ms. Comparison of simulations with and without time stepping showed very small differences in APD (0.2%) and CV (0.07%), indicating the suitability of this scheme. No-flux boundary conditions were imposed at each tissue edge by setting the gradient of membrane voltage normal to the edge to be zero at boundary points.

3.3. Dynamic properties of the model

To examine the effects of the different components of ischaemia on the tissue model, we measured how combinations of elevated $[K^+]_o$ and lowered $[ATP]_i$ influenced APD and CV restitution, effective refractory period (ERP), the range of CV, and the tissue wavelength, which is the product of CV and ERP.

To make these measurements, a thin strip of tissue with dimensions of 5 × 200 grid points (0.125 × 5 cm) was used, with an S1S2 stimulus protocol. Each stimulus was delivered by applying a stimulus current of −52.0 pA pF^{-1} to a small region of tissue at one end of the tissue strip with dimensions of 5 × 3 grid points for 1 ms. The S2 cycle length was varied between 1000 ms and 100 ms, and the minimum S2 that would support a propagating action potential was determined with a resolution of 5 ms. Each S2 stimulus was delivered following six S1 stimuli with a cycle length of 1000 ms. Following each S2, the tissue was restored to its initial state before the next S1S2 sequence. The timing of each action potential upstroke and downstroke was identified at two points located 5 grid points from each end of the strip, and these measurements were used to calculate DI, APD, and CV.

3.4. Tissue model and simulated re-entry

The computational cost of cardiac tissue simulations can be high, especially with a range of parameters to vary. It was therefore not practical to simulate the effect of progressive ischaemia over the period of 180 s as in our human data. To examine how combinations of elevated $[K^+]_o$ and reduced $[ATP]_i$ influenced re-entry, we ran tissue simulations with an initial condition that was either a single re-entrant wave, or multiple re-entrant waves.

These simulations were done using a 2D square tissue sheet with dimensions of 1000 × 1000 grid points. For re-entry with a single spiral as the initial condition, an Archimedian spiral was imposed by setting the cell model variables at grid points lying on concentric circles to a complete action potential cycle (Biktashev and Holden, 1998). For re-entry with multiple wavelets as an initial condition, we ran a simulation with the TP06 model changed to the values that give an APD restitution curve slope of 1.8 described in Table 2 of the TP06 paper (Ten Tusscher and Panfilov, 2006). These values resulted in breakup of the initial spiral wave, and after 4 s of simulated activity we stored the full set of cell model state variables at each grid point. These stored values were then used as the initial condition. The number of PS in these simulations was determined by transforming the simulated voltage into phase using a time delay of 20 ms, and phase singularities were identified by the method of topological charge (Clayton et al., 2006; Bray and Wikswo, 2002).

One possible explanation for the increase in PS and wavefronts observed in our clinical data (Fig. 1b and c) is tissue heterogeneity. Data from studies in animal hearts suggest that during long duration VF the coefficient of variation of APD increases (Huizar et al., 2007). There are several possible types of heterogeneity that could account for this effect including regional differences in $I_{K,ATP}$ and other ion channels (Weiss et al., 2009; Tice et al., 2007), as well as regional differences in $[K^+]_o$ accumulation (Coronel et al., 1988).

We examined the effect of heterogenous $[K^+]_o$ by dividing the tissue sheet into regions with different values of $[K^+]_o$ and repeating simulations with multiple wavelet re-entry as an initial condition. We examined three different types of heterogeneity, with different shape and size; first, a circular region with a diameter of 700 grid points where $[K^+]_o$ had a lower value than the surrounding tissue; second, a square region with a side of length 500 grid points where $[K^+]_o$ had a lower value than the surrounding tissue; and third, 16 equally sized regions in the form of a chessboard, where $[K^+]_o$ took on one of two values in alternate squares. Three pairs of values were used for $[K^+]_o$; 5.4 and 7.0 mM, 5.4 and 9.0 mM, and 7.0 and 9.0 mM. We used a similar scheme to examine the effect of heterogeneity in $I_{K,ATP}$ activation. Heterogeneous $I_{K,ATP}$ activation was produced by regional differences in $[ATP]_i$ of 6.8 mM and 6.0 mM.

4. Results

4.1. Simulated ischaemia and restitution

Fig. 2 shows the effect of reduced $[ATP]_i$ and elevated $[K^+]_o$ on APD restitution (Fig. 2a and d), CV restitution (Fig. 2b and e), and action potential shape (Fig. 2c and f) in our model. The effect of

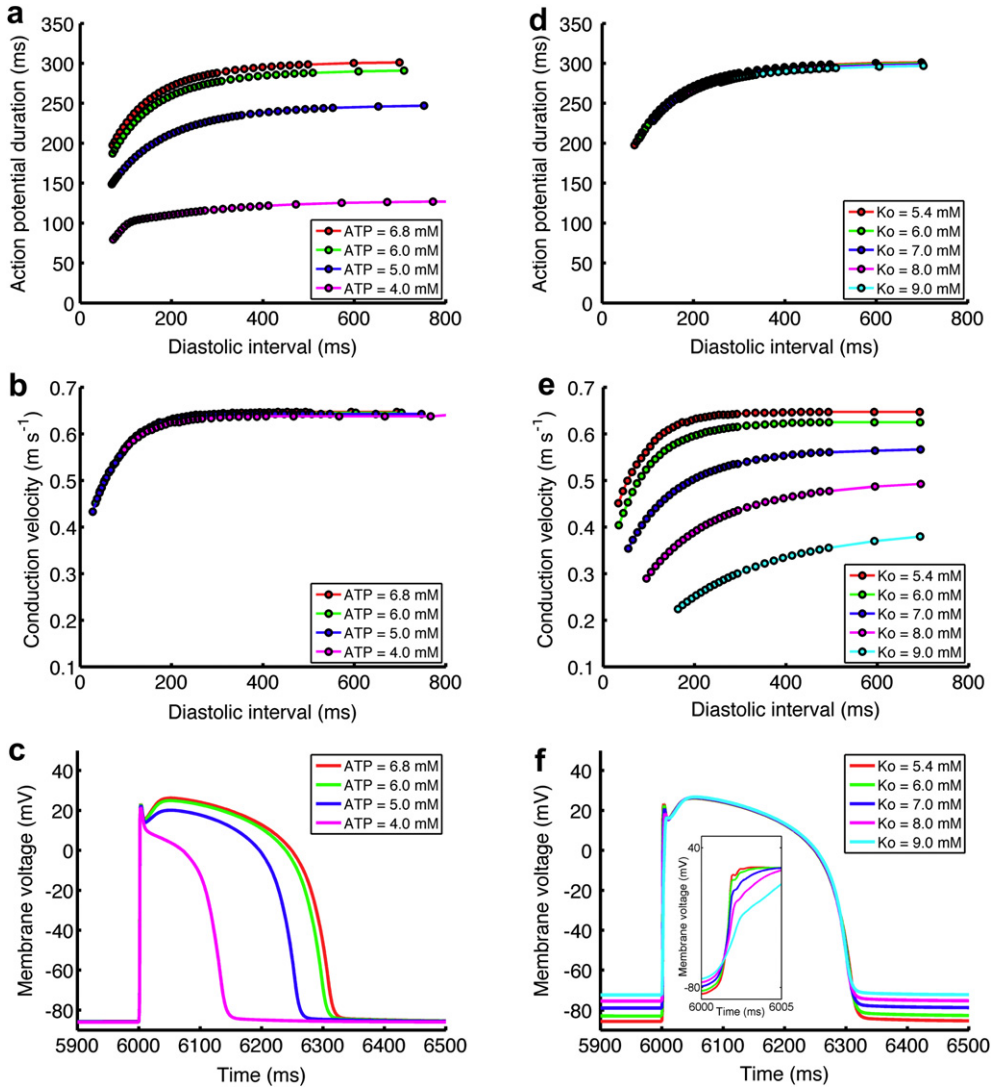

Fig. 2. (colour in print and on web) Effect of increased $[ATP]_i$ and decreased $[K^+]_o$ on APD restitution (a,d), CV restitution (b,e), and action potential shape (c,f).

reducing $I_{Ca.L}$ to 80% was to reduce APD by around 15 ms with no effect on CV. Since this effect was small compared to reduced $[ATP]_i$ and elevated $[K^+]_o$, these results are not shown and changes to $I_{Ca.L}$ were discounted from later studies.

The main features of the restitution curves in Fig. 2 are shown in Fig. 3, where we illustrate the effect of reduced $[ATP]_i$ and elevated $[K^+]_o$ on ERP and APD at long cycle lengths in Fig. 3a and d respectively. Fig. 3b and e show how the changes in ERP influence the tissue wavelength, which is the product of ERP and CV. Two values for CV are plotted in Fig. 3c and f, the larger value is the CV at long cycle length, and the smaller value is the minimum value of CV.

Decreasing $[ATP]_i$ activated $I_{K,ATP}$, which increased the total outward current during repolarisation, shortened APD and ERP (Fig. 3a), and hence reduced wavelength (Fig. 3b). Reduced $[ATP]_i$ acted to flatten the APD restitution curve (Fig. 2a), but had little effect on CV. In contrast to the effect of decreased $[ATP]_i$, elevated $[K^+]_o$ had little effect on APD (Fig. 2d), but acted to increase ERP (Fig. 3d), reduce CV (Fig. 2e and Fig. 3f), with a modest decrease in wavelength (Fig. 3e). The reduced CV can be attributed to increased (less negative) resting potential in tissue with elevated $[K^+]_o$. This change reduces the magnitude of the inward Na^+ current during depolarisation, in turn reduces the rate of change of membrane voltage during the action potential upstroke (shown in the inset in Fig. 2f), and hence acts to reduce CV.

4.2. Simulated re-entry in normal and ischaemic tissue

With a single re-entrant wave as the initial condition, all combinations of $[ATP]_i$ and $[K^+]_o$ resulted in stable re-entry. Table 1 shows the average period of re-entry for different combinations of $[ATP]_i$ and $[K^+]_o$, and includes the corresponding activation frequency. The reduced CV and increased ERP resulting from elevated $[K^+]_o$ acts to increase the period of re-entry, and hence decrease activation rate. In contrast, the reduced ERP and unchanged CV resulting from decreased decreased $[ATP]_i$ acts to decrease the period of re-entry and hence to increase activation rate.

In normal tissue, we found stable re-entry with a mean period of 222 ms, corresponding to a dominant frequency of 4.5 Hz, which is close to the initial value of mean dominant frequency found in our clinical data and shown in Fig. 1a. Increasing $[K^+]_o$ to 7.0 and 9.0 mM resulted in stable re-entry with an increased mean period of 313 and 497 ms respectively. These increases in period were qualitatively consistent with the fall in dominant frequency we

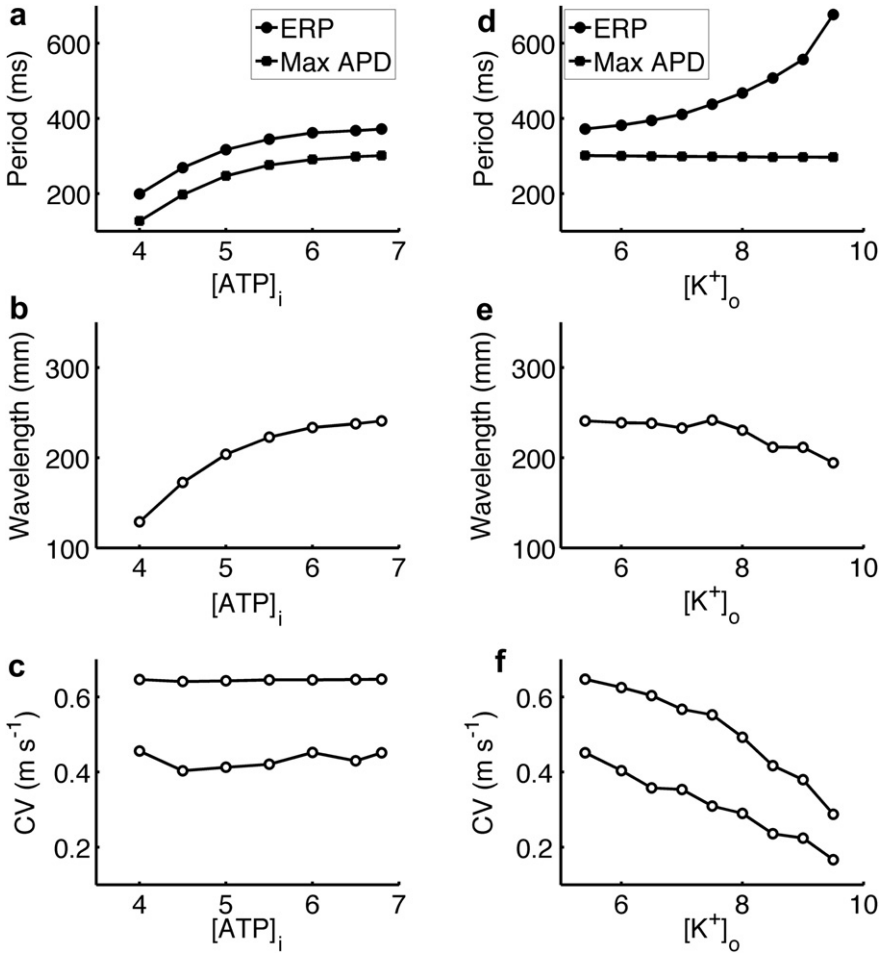

Fig. 3. Effect of increased $[ATP]_i$ and decreased $[K^+]_o$ on APD at long cycle length and ERP (a,d), wavelength (b,e), and CV at long and short cycle length (c,f).

observed in our clinical data during ischaemia (Fig. 1a). The quantitative difference may result from the fact that the data were obtained from the surface of 3D tissue, whereas the simulations were in a 2D tissue sheet, and this issue is discussed in more detail in Section 5.3.

The flattening of APD restitution and prolonging of ERP resulting from reduced $[ATP]_i$ and elevated $[K^+]_o$ would be expected to increase the stability of re-entry in ischaemic tissue. We examined this idea by using multiple wavelet re-entry as an initial condition for simulations with reduced $[ATP]_i$ and elevated $[K^+]_o$. Fig. 4 shows a snapshot of the initial condition, and snapshots of membrane voltage in the 2D tissue sheet after 2 s of simulated activity. The top row shows tissue with normal $[ATP]_i$ of 6.8 mM, and normal $[K^+]_o$ of 5.4 mM (left), elevated $[K^+]_o$ 7.0 mM (middle), and elevated $[K^+]_o$ 9.0 mM (right). The second and third rows show corresponding simulations with $[ATP]_i$ reduced to 6.0 mM (middle) and 4.0 mM (bottom).

Table 1
Average period of spiral wave re-entry in simulations with different combinations of $[ATP]_i$ and $[K^+]_o$. The figures in brackets indicate the corresponding frequency.

$[ATP]_i$ (mM)	$[K^+]_o$ (mM)		
	5.4	7.0	9.0
6.8	221.9 ms (4.5 Hz)	312.9 ms (3.2 Hz)	497.0 ms (2.0 Hz)
6.0	214.9 ms (4.6 Hz)	281.9 ms (3.5 Hz)	471.3 ms (2.1 Hz)
4.0	147.2 ms (6.8 Hz)	203.1 ms (4.9 Hz)	412.5 ms (2.4 Hz)

For normal tissue with $[ATP]_i$ of 6.8 mM and $[K^+]_o$ 5.4 mM the multiple wavefronts coalesced into a more stable pattern, but with intermittent wavebreak. With reduced $[ATP]_i$ and elevated $[K^+]_o$ there was a greater tendency of the multiple wavelets to stabilise into a pattern with a few persistent re-entrant waves. With elevation of $[K^+]_o$ to 9.0 mM and $[ATP]_i$ of both 6.0 and 4.0 mM re-entry was quickly extinguished. Fig. 5 shows how the number of PS changed throughout these simulations, and emphasises the stabilising effect of reduced $[ATP]_i$ and increased $[K^+]_o$. These findings indicate that the overall effect of global ischaemia with modest elevation of $[K^+]_o$ is to stabilise multiple wavelet VF, reducing the number of PS and wavefronts but not always extinguishing re-entrant activity. Our model indicates that reduced $[ATP]_i$ and increased $[K^+]_o$ suppress wavebreak and the creation of new PS, but these observations are not consistent with the steady increase in PS and wavefronts we observed in our clinical data (Fig. 1b and c).

4.3. Simulated re-entry with tissue heterogeneity

Fig. 6(a) shows the number of PS in each simulation with heterogeneity in $[K^+]_o$, and Fig. 6(b) the number of PS in the simulations with heterogeneous $[ATP]_i$. The top row of Fig. 6(s) shows results for tissue with $[ATP]_i$ of 6.8 mM and $[K^+]_o$ of 5.4 and 7.0 mM (left), 5.4 and 9.0 mM (middle), and 7.0 and 9.0 mM (right). The second and third rows show corresponding simulations with $[ATP]_i$ reduced to 6.0 mM (middle) and 4.0 mM (bottom). For simulations with heterogeneous $[K^+]_o$ of 7.0/9.0 mM, and

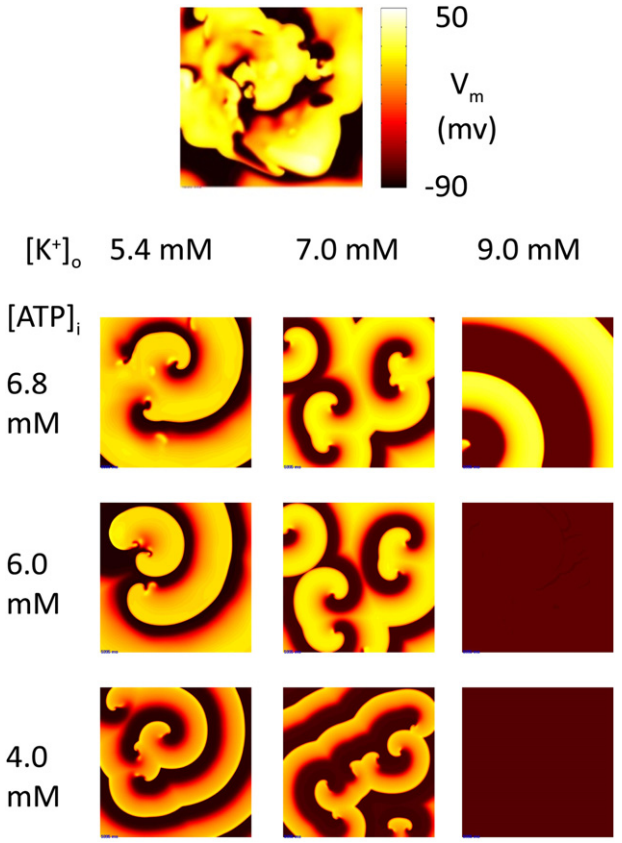

Fig. 4. (colour on web) Snapshots of re-entry in models with different combinations of $[ATP]_i$ and $[K^+]_o$. Each snapshot shows membrane voltage encoded using the intensity scheme shown in the top panel, 2 s after initiation with multiple wavelet re-entry as also shown in the top panel.

5.4/9.0 mM, and $[ATP]_i$ of either 6.8 mM or 6.0 mM, either a stable activation pattern or termination of re-entry developed within the first 2 s of simulation. The overall pattern is similar to the uniform tissue simulations shown in Figs. 4 and 5, but the time taken to either reach a stable activation pattern or to terminate was longer with heterogeneous $[K^+]_o$ than in uniform tissue, indicating that the destabilising effects of heterogeneity act to oppose the stabilising effects of elevated $[K^+]_o$. With heterogeneity in $[ATP]_i$, Fig. 6(b) shows that the number of PS gradually decreased over 2 s for a normal value of $[K^+]_o$, with a rapid stabilisation of the activation pattern with $[K^+]_o$ of 7.0 mM and rapid termination for $[K^+]_o$ of 9.0 mM.

Taken together, these results indicate that the overall shape of heterogeneity has little effect on the overall behaviour. Although heterogeneity acts to sustain wavebreak, the stabilising effect of elevated $[K^+]_o$ and reduced $[ATP]_i$ in our model is greater.

5. Discussion

In this paper we have sought to illustrate one approach for interaction between experiments and models using our on-going research on the effects of global cardiac ischemia on the organisation of VF in the human heart. We have shown that even modelling with simplified tissue geometry and a basic description of the cellular effects of ischemia can explain the decrease in VF activation rate observed in our experimental studies. However we have found that a model based investigation of wavebreak and PS dynamics is a more challenging problem, which requires closer interaction between experimental and modelling studies.

5.1. Relative effects of different components of ischaemia

In our model, reduced $[ATP]_i$ acted to decrease APD and ERP, while elevated $[K^+]_o$ acted to increase ERP and wavelength, and that elevated $[K^+]_o$ acted to reduce CV. The relative effect of reduced $I_{Ca,L}$ associated with acidosis was small, and overall these results are is in agreement with experimental studies (Kodama et al., 1984).

The reduction of APD associated with reduced $[ATP]_i$ is within the range that would be expected from other studies using the same cell model (Nickerson and Buist, 2008), and from other studies where $I_{K,ATP}$ has been included to simulate the effects of anoxia (Ferrero et al., 1996; Shaw and Rudy, 1997). The formulation for $I_{K,ATP}$

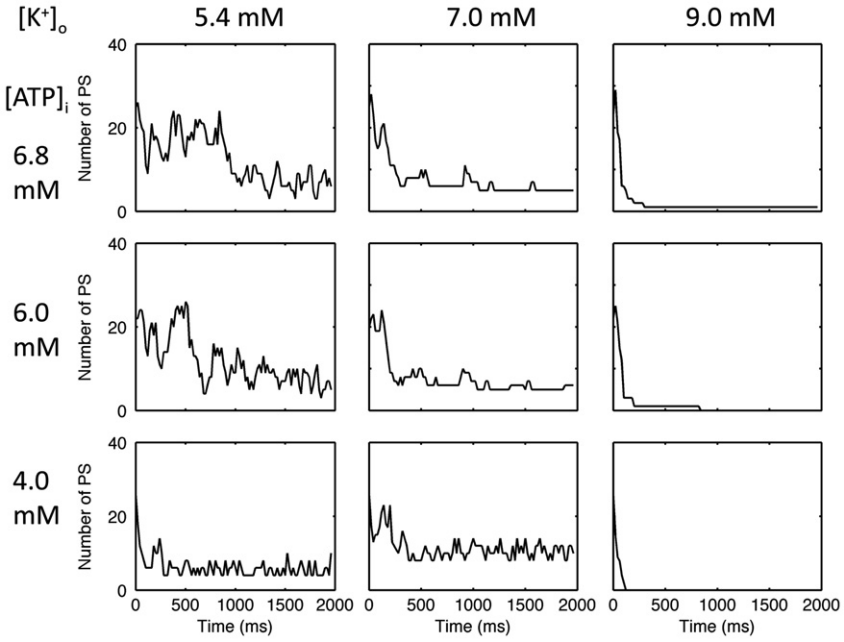

Fig. 5. Time series showing the number of PS present in the simulations shown in Fig. 4.

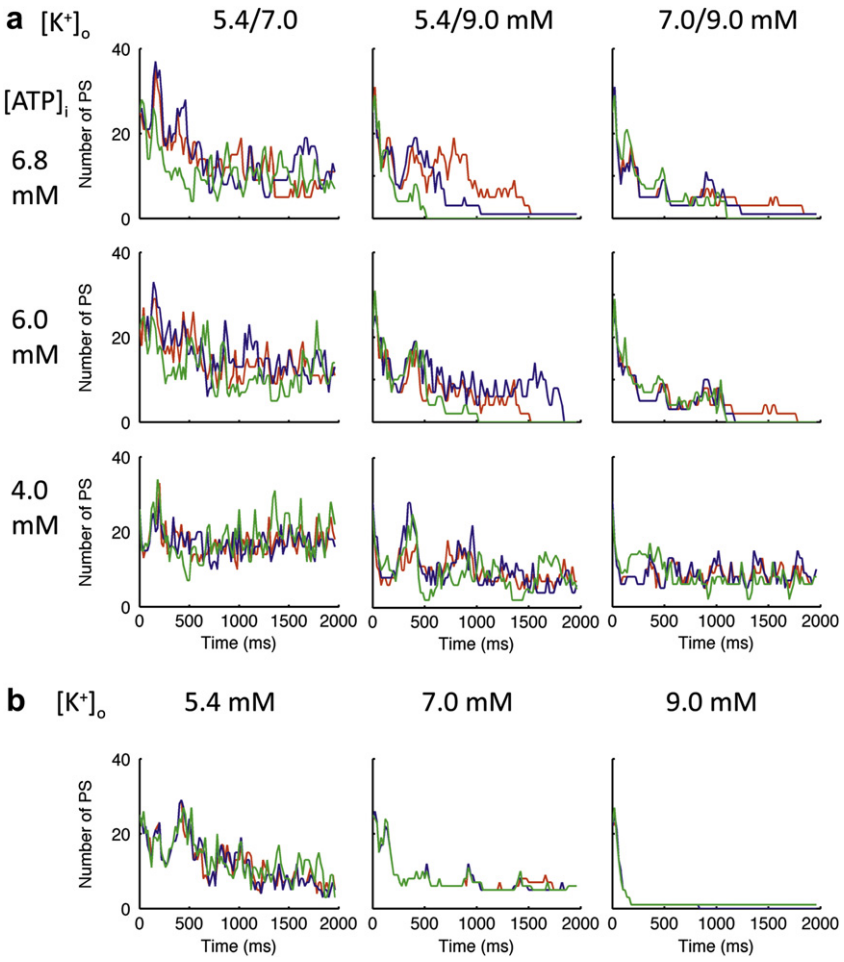

Fig. 6. (colour in print and on web) Time series showing the number of PS present in simulations with (a) heterogeneity in $[K^+]_o$, and (b) heterogeneity in $[ATP]_i$. Red indicates simulations with single circular heterogeneity, blue single square heterogeneity, and green 4 × 4 square heterogeneity.

has an influence on the APD changes that are produced (Nickerson and Buist, 2008), and an important future avenue is to develop models of $I_{K,ATP}$ that are based on data from human ventricular myocytes. In this study we reduced $[ATP]_i$ to a minimum value of 4.0 Mm which although only slightly lower than values used in similar simulation studies (Rodríguez et al., 2004), is a lower value than might be expected for around 3 min of ischaemia.

Experimental studies in the in-situ human heart indicate that 3 min of ischaemia reduces ventricular APD from around 256 ms−189 ms, and increases ERP from 256 to 348 ms (Sutton et al., 2000). A similar period of ischaemia acts to reduce CV transverse to fibres from 0.48 to 0.32 m s^{-1}, with an even greater reduction of transmural CV from 0.51 to 0.26 m s^{-1}. These values fit within the mid-range of our model findings (Fig. 3).

The increase in ERP and reduction in CV associated with elevated $[K^+]_o$ is what would be expected from experimental studies (Kodama et al., 1984; Wilde et al., 1988). Both changes are associated with a change in resting potential resulting from the altered Nernst potential for K^+, which acts to reduce the magnitude of I_{Na} during depolarisation, which in turn reduces dV/dt during the action potential upstroke (Fig. 2f) and hence reduces CV. The change in resting potential also slows the recovery of excitability, which accounts for the development of post repolarisation refractoriness (Shaw and Rudy, 1997).

Both experimental (Kodama et al., 1984) and modelling (Shaw and Rudy, 1997) studies indicate that elevated $[K^+]_o$ can be associated with a decrease in APD, but we only observed a very small change. In the TP06 model, elevated $[K^+]_o$ shifts the voltage dependence of each K^+ current and increases (makes less negative) the cell resting potential. In addition elevated $[K^+]_o$ increases the conductance of the rapidly inactivating K^+ channel I_{Kr}, and increases flow through the Na^+/K^+ exchanger. For the parameters used in our simulations, these effects tended to act in opposition, so for example the increase in conductance of the rapidly inactivating K^+ channel I_{Kr} was opposed by the shift in voltage dependence resulting from the change in Nernst potential for K^+.

5.2. Role of tissue heterogeneity

Structural and functional tissue heterogeneity is known to be a potent source of wavebreak and to favour the breakup of re-entry (Choi et al., 2001; Clayton and Holden, 2005; Moe et al., 1964). It is therefore not surprising that imposing regional differences acted to prolong periods of wavebreak despite the stabilising effects of simulated ischaemia. However, regional differences in $[K^+]_o$ and $I_{K,ATP}$ activation are only two sources of heterogeneity that could explain the continuing wavebreak in our experimental studies. Others include the effects of tissue geometry and the fibre-sheet structure of the ventricular wall (Caldwell et al., 2009), local preconditioning and the effects of pre-existing cardiovascular disease, as well as regional differences in the response to ischaemia within

the ventricular wall (Kong et al., 2009; Michailova et al., 2007; Tice et al., 2007; Weiss et al., 2009).

The key finding from the present study is that heterogeneity acts in opposition to the stabilising effects of ischaemia and especially of $[K^+]_o$ accumulation, and whether wavebreak increases or decreases during ischaemia will depend on the relative importance of these mechanisms. Introducing heterogeneity into our 2D tissue model did not result in sustained wavebreak with ischaemia, and so the explanation for our findings in human VF must arise from other mechanisms that were not included in this model, and these are discussed below.

5.3. Interaction of our model and data from human VF

Our experimental data (Fig. 1) show that the main effects of global myocardial ischaemia on VF in the human heart are an initial decrease in DF followed by a steady fall, and a steady increase in the number of PS and wavefronts.

The fall in DF is consistent with a gradual reduction in CV and increase in ERP associated with the effects of $[K^+]_o$ accumulation. However the activation frequency during simulated re-entry in our 2D model of normal and ischaemic tissue was lower than the dominant frequencies observed in the human heart. This is valuable input from experiment to model which can be used for adjusting the model to reconstruct ischaemia, and one possible explanation for this difference is the more complex surface activation patterns that can result from simulated VF in 3D tissue compared to a 2D tissue sheet. In the present study we have not investigated the effect of simulated reflow, which had a rapid and dramatic effect on activation rate that is likely to be the effect of K^+ washout.

Accounting for the sustained wavebreak that we observed during ischaemia has been more difficult. The number of PS observed may depend on how they are detected, as well as experimental factors including the electrode spacing and the processing including interpolation procedures. The human ventricles are 3D tissue with detailed geometry and structure (Caldwell et al., 2009), rather than the 2D tissue sheets simulated in the present study. There are also important differences between 2D and 3D re-entry (Clayton et al., 2006; Clayton, 2009).

Most of the changes in the model resulting from simulated ischaemia would act to stabilise re-entry, and this effect was shown clearly in Figs. 4 and 5. The results shown in Fig. 6 indicate that tissue heterogeneity can act to oppose that stabilising effects of ischaemia, and so the effect of heterogeneity is one potential explanation for the sustained wavebreak observed in our experimental data. However other mechanisms of wavebreak can operate in 3D tissue, such as negative filament tension associated with reduced excitability (Biktashev et al., 1994) and these may also play an important role, together with the structure and shape of the ventricular wall, as well as transmural heterogeneities in action potential shape and duration, and regional differences in the response of ATP sensitive K^+ channels (Michailova et al., 2007; Weiss et al., 2009). Future work will extend our simulations into 3D to examine the contribution of these different types of heterogeneity to wavebreak during human VF.

A more general issue arising from this study is the difficulty of establishing reasonable parameter values for simulating ischaemia at the cell scale. Despite recent progress in understanding parameter sensitivity in cardiac cell models (Romero et al., 2009), there is still an urgent need for tools to enable prediction of the tissue scale effects of cell scale parameter changes such as those that are associated with ischaemia.

Related to this is the suitability of cardiac cell models for representing the behaviour of cardiac cells and tissue during the natural progresion of ischaemia, which occurs over a period of minutes. Our simulations represent snapshots of activity, and while we were able to choose initial conditions to simulate the effect of ischaemia on multiple wavelet re-entry, longer simulations that reconstruct the gradual development of ischaemia over several minutes would enable a closer link between model and experiment. This is a difficult challenge for future studies not only because of the high computational cost, but also because the time course of changes in $[K^+]_o$, $[ATP]_i$, and pH during ischaemia in the human heart need to be characterised.

5.4. Limitations

In our experimental data, our observations were limited to the ventricular epicardium, and do not take into account differences in the sensitivity to ischaemia and VF dynamics between epicardium and endocardium that have been reported, and other parts of the heart such as the Purkinje system that may play an important role in VF maintenance (Tabereaux and Dosdall, 2009). During surgery the heart is exposed, and so it is possible that temperature variations may be important. However, we observed no significant differences in DF between the exposed anterior surface and the posterior epicardium, and in a previous study using a similar patient model (Taggart et al., 1988) temperature changes of less than 0.50 °C were observed during the first minute of cardiopulmonary bypass, so it is unlikely that temperature exerts a significant effect.

The model that we have used in this study is a greatly simplified model not only of global cardiac ischaemia, but also of human ventricular tissue structure and geometry. We have already discussed many of the important assumptions and limitations in Section 2.3. Our representation of ischaemia neglects the detailed mechanisms by which ischaemia modifies cell metabolism (Michailova et al., 2007; Terkildsen et al., 2007), as well as regional differences in ion channel expression (Weiss et al., 2009). A further simplification is that we have not considered the effect of prolonged ischaemia on gap junction conductance, which may favour wavebreak (De Groot and Coronel, 2004). Our models of tissue heterogeneity employ arbitrary and regular patterns of regional differences, whereas the actual heterogeneities may be much more irregular and patchy. Finally, our model does not take into account the effect of mechanics, which may also influence the stability of re-entry (Keldermann et al., 2010).

6. Conclusions

Our simplified model of human ventricular tissue with global ischaemia has shown elevated $[K^+]_o$ and decreased $[ATP]_i$ act to slow conduction velocity, increase refractoriness, reduce APD, and flatten APD restitution. All of these changes act to stabilise re-entry. However, this stabilising effect can be reduced by the effects of regional differences in $[K^+]_o$, and $I_{K,ATP}$ activation which act to create new wavebreaks. However, more detailed models that describe 3D tissue structure and heterogeneity are needed to fully explain continuing wavebreak we have observed during VF in the human heart with global myocardial ischaemia.

Editors' note

Please see also related communications in this issue by Aguado-Sierra et al. (2011) and Camara et al. (2011).

Acknowledgements

M. P. Nash is supported by a James Cook Fellowship administered by the Royal Society of New Zealand on behalf of the New Zealand Government. P Taggart acknowledges support from the UK Medical Research Council. A. V. Panfilov was partially supported by

the Institut des Hautes Etudes Scientifiques (Bures-sur-Yvett, France) and the James Simons Foundation. We are grateful to I. Kazbanov for valuable discussions on the results of simulations.

References

Aguado-Sierra, J., Krishnamurthy, A., Villongco, C., Howard, E., Chuang, J., 2011. Patient-specific modeling of dyssynchronous heart failure: a case study. Progress in Biophysics and Molecular Biology 107, 147–155.

Befroy, D.E., Powell, T., Radda, G.K., Clarke, K., 1999. Osmotic shock: modulation of contractile function, pH_i, and ischemic damage in perfused guinea pig heart. American Journal of Physiology (Heart and Circulatory Physiology) 276, H1236–H1244.

Biktashev, V.N., Holden, A.V., Zhang, H., 1994. Tension of organizing filaments of scroll waves. Philosophical Transactions of the Royal Society A: Mathematical Physical and Engineering Sciences 347, 611–630.

Biktashev, V.N., Holden, A.V., 1998. Re-entrant waves and their elimination in a model of mammalian ventricular tissue. Chaos, 48–56.

Bradley, C.P., Clayton, R.H., Nash, M.P., Mourad, A., Hayward, M., Paterson, D.J. & Taggart, P. Human ventricular fibrillation during global ischemia and reperfusion: paradoxical changes in activation rate and wavefront complexity. Circulation Arrhythmia and Electrophysiology, in press.

Bray, M.-A., Wikswo, J.P., 2002. Use of topological charge to determine filament location and dynamics in a numerical model of scroll wave activity. IEEE Transactions on Biomedical Engineering. 49, 1086–1093.

Caldwell, B.J., Trew, M.L., Sands, G.B., Hooks, D.A., LeGrice, I.J., Smaill, B.H., 2009. Three distinct directions of intramural activation reveal nonuniform side-to-side electrical coupling of ventricular myocytes. Circulation Arrhythmia and Electrophysiology 2, 433–440.

Camara, O., Sermesant, M., Lamata, P., Wang, L., Pop, M., 2011. Inter-model consistency and complementarity: learning from ex-vivo imaging and electrophysiological data towards an integrated understanding of cardiac physiology. Progress in Biophysics and Molecular Biology 107, 122–133.

Carmeliet, E., 1999. Cardiac ionic currents and acute ischemia: from channels to arrhythmias. Physiological Reviews 79, 917–1017.

Choi, B.R., Liu, T., Salama, G., 2001. The distribution of refractory periods influences the dynamics of ventricular fibrillation. Circulation Research 88, e49–e58.

Clayton, R.H., 2009. Influence of cardiac tissue anisotropy on re-entrant activation in computational models of ventricular fibrillation. Physica D: Nonlinear Phenomena 238, 951–961.

Clayton, R.H., Bernus, O., Cherry, E.M., Dierckx, H., Fenton, F.H., Mirabella, L., Panfilov, A.V., Sachse, F.B., Seemann, G., Zhang, H., 2011. Models of cardiac tissue electrophysiology: progress, challenges and open questions. Progress in Biophysics and Molecular Biology 104, 22–48.

Clayton, R.H., Zhuchkova, E., Panfilov, A.V., 2006. Phase singularities and filaments: simplifying complexity in computational models of ventricular fibrillation. Progress in Biophysics and Molecular Biology. 90, 378–398.

Clayton, R.H., Holden, A.V., 2005. Dispersion of cardiac action potential duration and the initiation of re-entry: a computational study. BioMedical Engineering OnLine 4, 11.

Coronel, R., Fiolet, J.W., Wilms-Schopman, F.J., Schaapherder, A.F., Johnson, T.A., Gettes, L.S., Janse, M.J., 1988. Distribution of extracellular potassium and its relation to electrophysiologic changes during acute myocardial ischemia in the isolated perfused porcine heart. Circulation 77, 1125–1138.

De Groot, J.R., Coronel, R., 2004. Acute ischemia-induced gap junctional uncoupling and arrhythmogenesis. Cardiovascular Research 62, 323–334.

Fenton, F.H., Cherry, E.M., Hastings, H.M., Evans, S.J., 2002. Multiple mechanisms of spiral wave breakup in a model of cardiac electrical activity. Chaos 12, 852–892.

Ferrero, J.M.J., Trenor, B., Rodríguez, B., Saiz, J., 2003. Electrical activity and re-entry during acute regional ischaemia: insights from simulations. International Journal of Bifurcation and Chaos 13, 3703–3716.

Ferrero, J.M.J., Saiz, J., Ferrero, J.M., Thakor, N.V., 1996. Simulation of action potentials from metabolically impaired cardiac myocytes. Role of ATP-sensitive K^+ current. Circulation Research. 79, 208–221.

Garny, A., Noble, D., Kohl, P., 2005. Dimensionality in cardiac modelling. Progress in Biophysics and Molecular Biology 87, 47–66.

Grandi, E., Pasqualini, F.S., Bers, D.M., 2010. A novel computational model of the human ventricular action potential and Ca transient. Journal of Molecular and Cellular Cardiology 48, 112–121.

Huang, J., Rogers, J.M., Killingsworth, C.R., Singh, K.P., Smith, W.M., Ideker, R.E., 2004. Evolution of activation patterns during long-duration ventricular fibrillation in dogs. American Journal of Physiology (Heart and Circulatory Physiology) 286, H1193–H1200.

Huizar, J.F., Warren, M.D., Shvedko, A.G., Kalifa, J., Moreno, J., Mironov, S., Jalife, J., Zaitsev, A.V., 2007. Three distinct phases of VF during global ischemia in the isolated blood-perfused pig heart. American Journal of Physiology (Heart and Circulatory Physiology) 293, H1617–H1628.

Janse, M.J., Wit, A.L., 1989. Electrophysiological mechanisms of ventricular arrhythmias resulting from myocardial ischemia and infarction. Physiological Reviews 69, 1049–1162.

Jessen, M.E., Abd-Elfattah, A.S., Wechsler, A.S., 1996. Neonatal myocardial oxygen consumption during ventricular fibrillation, hypothermia, and potassium arrest. Annals of Thoracic Surgery 61.

Keldermann, R.H., Nash, M.P., Gelderblom, H., Wang, V.Y., Panfilov, A.V., 2010. Electromechanical wavebreak in a model of the human left ventricle. American Journal of Physiology (Heart and Circulatory Physiology) 299, H134–H143.

Keldermann, R.H., ten Tusscher, K.H.W.J., Nash, M.P., Bradley, C.P., Hren, R., Taggart, P., Panfilov, A.V., 2009. A computational study of mother rotor VF in the human ventricles. American Journal of Physiology (Heart and Circulatory Physiology) 296, H370–H379.

Keldermann, R.H., Ten Tusscher, K.H.W.J., Nash, M.P., Hren, R., Taggart, P., Panfilov, A.V., 2008. Effect of heterogeneous APD resitution on VF organization in a model of the human ventricles. American Journal of Physiology (Heart and Circulatory Physiology) 294, H764–H774.

Kodama, I., Wilde, A., Janse, M.J., Durrer, D., Yamada, K., 1984. Combined effects of hypoxia, hyperkalemia and acidosis on membrane action potential and excitability of guinea-pig ventricular muscle. Journal of Molecular and Cellular Cardiology 16, 247–259.

Kong, W., Ideker, R.E., Fast, V.G., 2009. Transmural optical measurements of V_m during long-duration ventricular fibrillation in canine hearts. Heart Rhythm 6, 796–802.

Li, L., Jin, Q., Huang, J., Cheng, K.-A., Ideker, R., 2008. Intramural foci during long duration fibrillation in the pig ventricle. Circulation Research 102, 1256–1264.

Mandapati, R., Asano, Y., Baxter, W.T., Gray, R., Davidenko, J., Jalife, J., 1998. Quantification of effects of global ischemia on dynamics of ventricular fibrillation in isolated rabbit heart. Circulation 98, 1688–1696.

Masse, S., Downar, E., Chauhan, V., Sevaptsidis, E., Nanthakumar, K., 2007. Ventricular fibrillation in myopathic human hearts: mechanistic insights from in vivo global endocardial and epicardial mapping. American Journal of Physiology (Heart and Circulatory Physiology) 292, H2589–H2597.

Masse, S., Farid, T., Dorian, P., Umapathy, K., Nair, K., Asta, J., Ross, J., Rao, V., Sevaptisidis, E., Nanthakumar, K., 2009. Effect of global ischemia and reperfusion during ventricular fibrillation in myopathic human hearts. American Journal of Physiology (Heart and Circulatory Physiology) 297, H1984–H1991.

Matsuoka, S., Sarai, N., Kuratomi, S., Ono, K., Noma, A., 2003. Role of individual ionic current systems in ventricular cells hypothesized by a model study. The Japanese Journal of Physiology. 53, 105–123.

Michailova, A., Lorentz, W., McCulloch, A., 2007. Modeling transmural heterogeneity of K(ATP) current in rabbit ventricular myocytes. American Journal of Physiology (Cell Physiology) 293, C542–C557.

Moe, G.K., Rheinboldt, W.C., Abildskov, J.A., 1964. A computer model of atrial fibrillation. American Heart Journal 67, 200–220.

Nanthakumar, K., Walcott, G.P., Melnick, S., Rogers, J.M., Kay, M.W., Smith, W.M., Ideker, R.E., Holman, W., 2004. Epicardial organization of human ventricular fibrillation. Heart Rhythm 1, 14–23.

Nash, M.P., Bradley, C.P., Sutton, P.M.I., Clayton, R.H., Kallis, P., Hayward, M.P., Paterson, D.J., Taggart, P., 2006a. Whole heart action potential duration restitution properties in cardiac patients: a combined clinical and modelling study. Experimental Physiology 91, 339–354.

Nash, M.P., Mourad, A., Clayton, R.H., Sutton, P.M., Bradley, C.P., Hayward, M., Paterson, D.J., Taggart, P., 2006b. Evidence for multiple mechanisms in human ventricular fibrillation. Circulation 114, 536–542.

Nickerson, D., Buist, M., 2008. Practical application of CellML 1.1: the integration of new mechanisms into a human ventricular myocyte model. Progress in Biophysics and Molecular Biology 98, 38–51.

Noble, D., 2002. The rise of computational biology. Nature Reviews Molecular Cell Biology 3, 459–463.

Qu, Z., Garfinkel, A., 1999. An advanced algorithm for solving partial differential equation in cardiac conduction. IEEE Transactions on Biomedical Engineering 46, 1166–1168.

Rodríguez, B., Tice, B.M., Eason, J.C., Aguel, F., Ferrero, J.M., Trayanova, N., 2004. Effect of acute global ischemia on the upper limit of vulnerability: a simulation study. American Journal of Physiology (Heart and Circulatory Physiology) 286, H2078–H2088.

Romero, L., Pueyo, E., Fink, M., Rodríguez, B., 2009. Impact of ionic current variability on human ventricular cellular electrophysiology. American Journal of Physiology (Heart and Circulatory Physiology) 297, H1436–H1445.

Shaw, R.M., Rudy, Y., 1997. Electrophysiologic effects of acute myocardial ischemia: a theoretical study of altered cell excitability and action potential duration. Cardiovascular Research 35, 256–272.

Sutton, P.M.I., Taggart, P., Opthof, T., Coronel, R., Trimlett, R., Pugsley, W., Kallis, P., 2000. Repolarisation and refractoriness during early ischaemia in humans. Heart (British Cardiac Society). 84, 365–369.

Tabereaux, P., Dosdall, D., 2009. Mechanisms of VF maintenance: wandering wavelets, mother rotors, or foci. Heart Rhythm 6, 405–415.

Taggart, P., Sutton, P.M.I., Boyett, M.R., Lab, M., Swanton, H., 1996. Human ventricular action potential during short and long cycles. Rapid modulation by ischaemia. Circulation 94, 2526–2534.

Taggart, P., Sutton, P., Treasure, T., Lab, M., O'Brien, W., Runnalls, M., Swanton, R.H., Emanuel, R.W., 1988. Monophasic action potentials at discontinuation of cardiopulmonary bypass: evidence for contraction–excitation feedback in man. Circulation 77, 1266–1275.

Ten Tusscher, K.H.W.J., Mourad, A., Nash, M.P., Clayton, R.H., Bradley, C.P., Paterson, D.J., Hayward, M.P., Panfilov, A.V., Taggart, P., 2009. Organization of ventricular fibrillation in the human heart: experiments and models. Experimental Physiology 94, 553–562.

Ten Tusscher, K.H.W.J., Noble, D., Noble, P., Panfilov, A., 2004. A model for human ventricular tissue. American Journal of Physiology (Heart and Circulatory Physiology) 286, H1573–H1589.

Ten Tusscher, K.H.W.J., Panfilov, A.V., 2006. Alternans and spiral breakup in a human ventricular tissue model. American Journal of Physiology (Heart and Circulatory Physiology) 291, H1088–H1100.

Terkildsen, J.R., Crampin, E.J., Smith, N.P., 2007. The balance between inactivation and activation of the Na+–K+ pump underlies the triphasic accumulation of extracellular K+ during myocardial ischemia. American Journal of Physiology (Heart and Circulatory Physiology) 293, H3036–H3045.

Tice, B.M., Rodríguez, B., Eason, J., Trayanova, N., 2007. Mechanistic investigation into the arrhythmogenic role of transmural heterogeneities in regional ischaemia phase 1A. Europace 9, vi46–vi58.

Venable, P.W., Taylor, T., Shibayama, J., Warren, M., Zaitsev, A.V., 2010. Complex structure of electrophysiological gradients emerging during long-duration ventricular fibrillation in canine heart. American Journal of Physiology (Heart and Circulatory Physiology) 299, H1405–H1418.

Walcott, G.P., Kay, G.N., Plumb, V.J., Smith, W.M., Rogers, J.M., Epstein, A.E., Ideker, R.E., 2002. Endocardial wave front organization during ventricular fibrillation in humans. Journal of the American College of Cardiology 39, 109–115.

Warren, M., Huizar, J.F., Shvedko, A., Zaitsev, A., 2007. Spatiotemporal relationship between intracellular Ca2+ dynamics and wave fragmentation during ventricular fibrillation in isolated blood-perfused pig hearts. Circulation Research 101, e90–101.

Weiss, D.L., Ifland, M., Sachse, F.B., Seemann, G., Dossel, O., 2009. Modelling of cardiac ischaemia in human myocytes and tissue including spatiotemporal electrophysiological mechanisms. Biomedizinische Technik 54, 107–125.

Weiss, J.N., Chen, P.S., Qu, Z., Karagueuzian, H.S., Garfinkel, A., 2000. Ventricular fibrillation: how do we stop the waves from breaking? Circulation Research 87, 1103–1107.

Weiss, J.N., Venkatesh, N., Lamp, S.T., 1992. ATP-Sensitive K+ channels and cellular K+ loss in hypoxic and ischaemic mammalian ventricle. The Journal of Physiology 447, 649–673.

Wiggers, C.J., 1940. The mechanism and nature of ventricular fibrillation. American Heart Journal 20, 399–412.

Wilde, A.A.M., Peters, R.J.G., Janse, M.J., 1988. Catecholamine release and potassium accumulation in the isolated globally ischemic rabbit heart. Journal of Molecular and Cellular Cardiology 20, 887–896.

Wu, T.-J., Lin, S.-F., Weiss, J.N., Ting, C.-T., Chen, P.-S., 2002. Two types of ventricular fibrillation in isolated rabbit hearts: importance of excitability and action potential duration restitution. Circulation 106, 1859–1866.

Wu, T.-J., Ong, J.J., Hwang, C., Lee, J.J., Fishbein, M.C., Czer, L., Trento, A., Blanche, C., Kass, R.M., Mandel, W.J., Karagueuzian, H.S., Chen, P.S., 1998. Characteristics of wave fronts during ventricular fibrillation in human hearts with dilated cardiomyopathy: role of increased fibrosis in the generation of reentry. Journal of the American College of Cardiology. 32, 187–196.